The FEBS Journal

FEBS PRESS science publishing by scientists

EDITOR'S CHOICE

Identification of a novel nucleophosmin-interaction motif in the tumor suppressor p14arf

Enrico Luchinat[1,2], Sara Chiarella[3,4], Mimma Franceschini[3,4], Adele Di Matteo[5], Maurizio Brunori[6], Lucia Banci[1,7] and Luca Federici[3,4]

1 CERM, Centro Risonanze Magnetiche, Università di Firenze, Italy
2 Dipartimento di Scienze Biomediche, Sperimentali e Cliniche – Università di Firenze, Italy
3 Ce.S.I.-MeT Centro di Scienze dell'Invecchiamento e Medicina Traslazionale, Università "G. d'Annunzio" di Chieti, Italy
4 Dipartimento di Scienze Mediche, Orali e Biotecnologiche – Università "G. d'Annunzio" di Chieti, Italy
5 Istituto di Biologia e Patologia Molecolari, Consiglio Nazionale delle Ricerche, Roma, Italy
6 Dipartimento di Scienze Biochimiche, "A. Rossi Fanelli" – Sapienza Università di Roma, Italy
7 Dipartimento di Chimica, Università di Firenze, Italy

Keywords
acute myeloid leukemia; ARF; B23; cancer target; NPM1; protein–protein interactions

Correspondence
L. Federici, CeSI-MeT and Dipartimento di Scienze Mediche, Orali e Biotecnologiche, Università "G. d'Annunzio" di Chieti, Via dei Polacchi, 66100, Chieti, Italy
Fax: +3908715410
Tel: +390871541558
E-mail: lfederici@unich.it
or
L. Banci, CERM Centro Risonanze Magnetiche and Dipartimento di Chimica, Università di Firenze, Via Luigi Sacconi 6, 50019, Sesto Fiorentino (Firenze), Italy
Fax: +390554574923
Tel: +390554574272/273
E-mail: banci@cerm.unifi.it

(Received 5 October 2017, revised 20 November 2017, accepted 20 December 2017)

doi:10.1111/febs.14373

The tumor suppressor p14arf interacts, in response to oncogenic signals, with the p53 E3-ubiquitin ligase HDM2, thereby resulting in p53 stabilization and activation. In addition, it also exerts tumor-suppressive functions in p53-independent contexts. The activities of p14arf are regulated by the nucleolar chaperone nucleophosmin (NPM1), which controls its levels and cellular localization. In acute myeloid leukemia with mutations in the *NPM1* gene, mutated NPM1 aberrantly translocates in the cytosol carrying with itself p14arf that is subsequently degraded, thus impairing the p14arf-HDM2-p53 axis. In this work we investigated the complex between these two proteins by means of NMR and other techniques. We identified a novel NPM1-interacting motif in the C-terminal region of p14arf, which corresponds to its predicted nucleolar localization signal. This motif recognizes a specific region of the NPM1 N-terminal domain and, upon binding, the two proteins form soluble high molecular weight complexes. By NMR, we identified critical residues on both proteins involved in the interaction. Collectively, our data provide a structural framework to rationalize the overall assembly of the p14arf-NPM1 supramolecular complexes. A number of p14arf cancer-associated mutations cluster in this motif and their effect on the interaction with NPM1 was also analyzed.

Introduction

The human p14arf tumor suppressor protein (p19arf in mice) arises from an alternative reading frame transcription of the *Ink4a* gene, also encoding a second tumor suppressor, the $p16^{Ink4a}$ protein [1,2]. The two proteins are transcribed from different promoters and share two of their three exons. This gene is frequently altered in

Abbreviations
AML, acute myeloid leukemia; CCSD, combined chemical shift differences; HDM2, human double minute 2; NOE, nuclear overhauser effect; NoLS, nucleolar localization signal; NPM1, nucleophosmin; SEC-MALS, size exclusion chromatography–multiangle light scattering.

tumors. Alterations include the loss of the *Ink4b–Arf–Ink4a* locus or of only the *Ink4a* exon Ib, which is specific for p14arf. Moreover, several mutations at exon II, encoding the C-terminal half of p14arf, were described [3,4]. They range from frameshift mutations, with the appearance of premature stop codons, to several missense mutations. The tumor spectrum of p14arf mutations is varied and includes: anaplastic meningioma, angiosarcoma, bladder adenocarcinoma, breast cancer, chronic myelogenous leukemia, colorectal carcinoma, T-cell acute lymphoblastic leukemia, and many others [5]. The tumor-suppressive importance of this protein is confirmed by the spontaneous development of tumors in mice knocked-out for the p14arf homologue p19arf as early as 8 weeks after birth [6].

P14arf is expressed at low levels and localized in the nucleoli of unstressed cells. However, its expression is strongly upregulated by oncogenic signals including E1A, Ras, c-Myc, E2F-1 and v-Abl [7]. Its classical activity as a tumor suppressor consists in the stabilization of p53 via a p14arf/human double minute 2 (HDM2)/p53 axis. HDM2 is the main E3-ubiquitin ligase of p53 and maintains p53 levels low in unstressed cells. When prompted by oncogenic signals, p14arf interacts with HDM2, liberating p53 from HDM2-mediated translocation and ubiquitination in the cytoplasm [8]. More recently a number of p53-independent tumor-suppressive functions have also been ascribed to p14arf [2].

Among the p14arf interaction partners, much interest has been devoted to nucleophosmin (NPM1). NPM1 is a nucleus-cytoplasmic shuttling chaperone, mainly localized in nucleoli, that plays crucial activities in ribosome maturation and export, DNA damage response, centrosome duplication and response to stress stimuli [9–11]. NPM1 is frequently overexpressed in solid tumors and is the subject of chromosomal translocations and mutations in hematological malignancies. Notably, NPM1 is the most frequently mutated protein in acute myeloid leukemia (AML) [12]. Mutations are always heterozygous and consist in frameshift insertions at the terminal exon of the gene, resulting in the unfolding of the C-terminal nucleic acid binding domain [13], the loss of the nucleolar localization signal (NoLS) and the appearance of a novel nuclear export signal (NES). Therefore, mutated NPM1 is aberrantly and stably delocalized in the cytosol of leukemic blasts [12].

In unstressed cells, NPM1 colocalizes with the tumor suppressor p14arf in the nucleolus, where they are found in high molecular weight complexes [14]. There is evidence that NPM1 sequesters p14arf into the nucleolus, impairing p14arf-HDM2 association and inhibiting p14arf-dependent p53 activation [15,16]. In response to cellular stress both NPM1 and p14arf relocalize in the nucleoplasm, where they may compete for binding to HDM2 [17]. Thus, the p14arf nucleoplasmic interaction with HDM2, that regulates the p53 cell-cycle checkpoint, depends on NPM1 localization. This is consistent with the loss of p14arf in leukemic blasts, due to its cytoplasmic translocation played by mutated NPM1, and subsequent degradation [18]. This mechanism leads to the inactivation of the p14arf/HDM2/p53 tumor suppressor pathway in the blasts despite p53 being always wild-type in this type of leukemia [19]. Therefore, the p14arf/NPM1 interaction surface has been proposed as a drug target for the treatment of AML with NPM1 mutation [20]. In fact, interfering with this interaction may rescue p14arf levels in leukemic blasts and activate the p53 pathway.

The interaction between mouse p19arf and NPM1 has been recently investigated [21]. It was shown that the N-terminal domain of NPM1 interacts with a p19arf-derived peptide consisting of the first six N-terminal residues. Previously, the structural properties of a peptide resembling the first 37 residues of p19arf were also determined, showing that it is intrinsically unstructured but able to form fibrillar-like structures when in complex with its HDM2-interacting epitope [22,23].

We decided to further investigate this interaction using, for the first time, human full-length p14arf (Fig. 1A). We show that isolated p14arf forms aggregates through its N-terminal region and that the NPM1 N-terminal domain (residues 16–123; Fig. 1A) exerts a chaperone activity against this phenomenon. Our data also indicate that the two proteins form soluble supramolecular complexes upon binding. Importantly, these are mediated by a second region of p14arf, in addition to the N-terminal segment, which we show to interact with the NPM1 N-terminal domain. This novel NPM1-interacting region is located in the C-terminal half of the protein, is rich in arginine residues and corresponds to the predicted NoLS of p14arf. We identified the residues involved on both sides by fluorescence and solution NMR spectroscopies. Importantly, this novel interaction region of p14arf is frequently deleted or mutated in cancer; therefore, we also analyzed the effect of p14arf cancer-associated mutations on the interaction with NPM1. We suggest that the NPM1 surface we have characterized here may be considered as a drug target in AML.

Results

Structural analysis of full-length p14arf

Structural information available so far on p14arf (Fig. 1A), or its mouse homologue p19arf, is limited

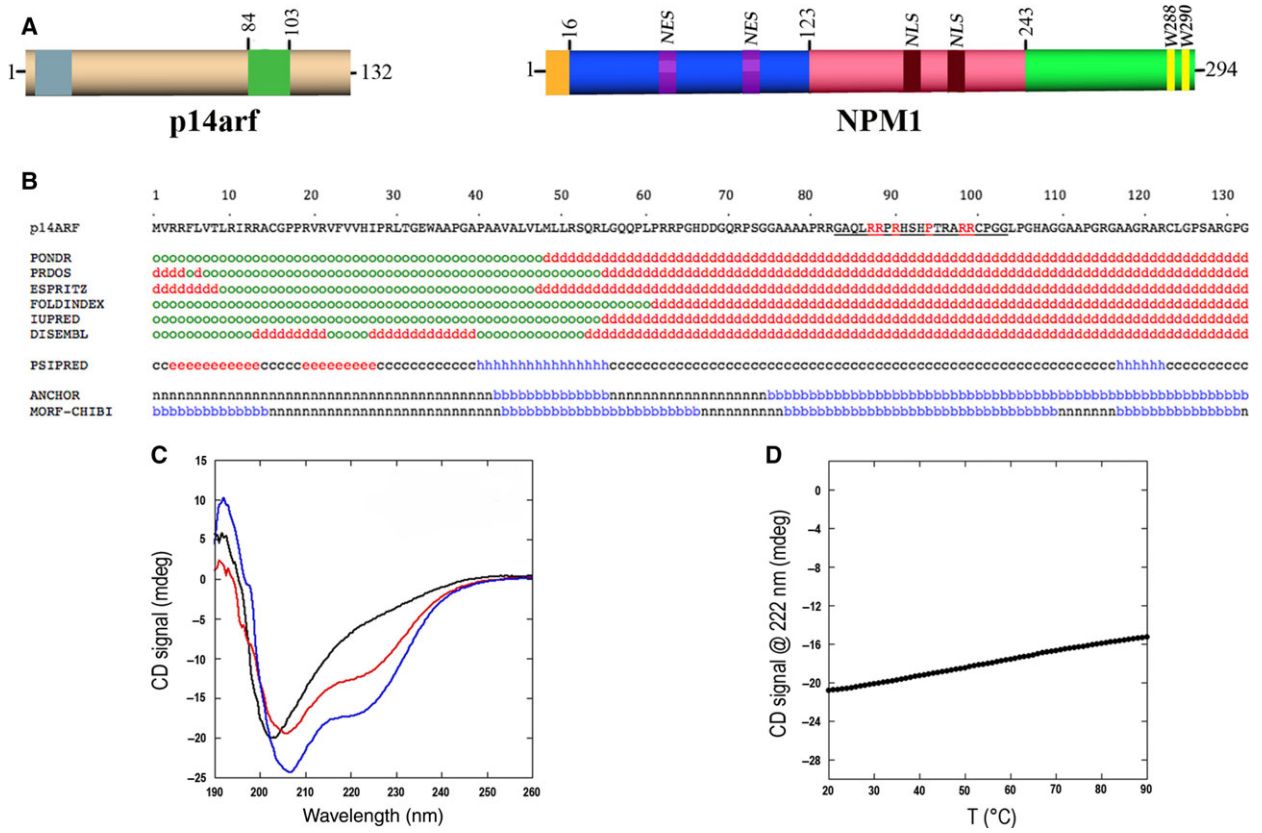

Fig. 1. Domain organization and analysis of p14arf secondary structure and disorder (A) p14arf consists of 132 residues; here the predicted NoLS (residues 84–103) is highlighted in green. Also shown, in cyan, the N-terminal tail of the protein, which was previously shown to interact with NPM1. NPM1 consists of a methionine-rich N-terminal tail (residues 1–15), a N-terminal domain (NPM1-Nter; 16–123), a central unstructured domain (residues 124–242) and a C-terminal nucleic acid binding domain (residues 243–294). The NES, nuclear localization signals (NLS) and the two tryptophan residues forming the NoLS are also highlighted. (B) Primary structure of human p14arf (132 residues). The underlined sequence corresponds to the putative NoLS as predicted by the NoD algorithm. Residues in red within this region are those that are found mutated in human cancers. Shown are predictions of protein disorder obtained with six different algorithms. (o) Stands for ordered and (d) for disordered residue. A secondary structure propensity prediction as calculated by PSIPRED is also shown, where (e) stands for strand, (h) stands for helix and (c) stands for coil. Two algorithms (ANCHOR and MORF-CHIBI) predict sites in intrinsically disordered protein prone to undergo interaction with globular proteins coupled to disorder-to-order transition: (n) stands for nonbinding while (b) stands for binding. As to the MORF-CHIBI prediction, residues with a MCW score higher than 0.75 were considered as binding prone. (C) CD spectra of full-length p14arf in the absence (black line) or in the presence of 20% (red) or 30% (blue) trifluoroethanol. (D) Thermal denaturation profile of full-length p14arf following the CD signal at 222 nm.

to the first 37 residues of the reference sequence. This segment of the protein is intrinsically disordered and able to interact with HDM2, forming fibril-like high molecular weight assemblies [22,23].

Figure 1B shows a preliminary bioinformatics analysis on the p14arf sequence, conducted using several order/disorder predictors. Interestingly, all of them suggest the presence of ordered regions in the N-terminal end of the sequence. To verify whether the N-terminal half of p14arf is indeed structured in the context of the entire protein, we expressed and purified the full-length construct. First, we analyzed this protein construct by far UV CD. Figure 1C,D show the CD spectrum of p14arf and its thermal denaturation, respectively. The shape of the spectrum is that typical of unstructured proteins, and the thermal denaturation profile suggests the absence of cooperative transitions from folded to unfolded species. However, a propensity to adopt helical structure in the presence of trifluoroethanol was also observed (Fig. 1C), partly consistent with PSIPRED secondary structure predictions that indicate the presence of alpha and beta structured regions in the N-terminal half of the protein (Fig. 1B). This behavior is also consistent with previous results obtained with the 37 aa N-terminal peptide from mouse p19arf [22].

The structural and dynamic properties of p14arf were investigated by NMR spectroscopy. At the protein concentration necessary for NMR analysis (100 μM), we observed a remarkably low solubility and abundant precipitation when the protein was in a non-denaturing buffer. Therefore, we analyzed p14arf in 20 mM phosphate buffer containing 4 M urea, a condition that we found sufficient to keep the protein in solution. ^{1}H- and ^{13}C-detected triple resonance NMR experiments, suitable for sequence-specific resonance assignment, were recorded on a sample of ^{13}C,^{15}N-labeled p14arf. Most of the crosspeaks arising from the N-terminal part of p14arf, comprising residues 1–56, were not detected in the triple resonance experiments and could not be assigned. Of the remaining 76 residues in the region between Gln57 and Gly132, 75 residues were assigned including 12 prolines (Fig. 2A). The loss of signal at the N-terminal region of p14arf suggests that this region is involved in the aggregation of the protein. Moreover, even in the moderately denaturing conditions of this experiment, p14arf could be in equilibrium between the free monomeric protein and soluble aggregates, resulting in signal disappearance in the N-terminal region due to either relaxation broadening or exchange broadening. The longitudinal (R_1), and transverse (R_2) ^{15}N-amide relaxation rates (Fig. 2B), the ^{15}N-nuclear overhauser effect (NOE; Fig. 2C) and the neighbor-corrected secondary structure propensity values calculated from the backbone chemical shifts (Fig. 2D) all indicate that the C-terminal fragment 57–132 of p14arf is intrinsically unstructured and does not have any secondary structure propensity in solution.

Notably, p14arf had been previously reported to be able to form oligomers, when ectopically overexpressed in H1299 cells [24]. Therefore, to get further insight into the aggregation propensity of p14arf in the absence of urea we employed a zero-angle light scattering (turbidity) assay. Figure 2E shows a tendency for a diluted sample of p14arf (0.3 μM) to aggregate when the temperature increases from 20 °C to higher values. Then, we measured the turbidity at 37 °C and at varying protein concentrations, showing that the aggregation propensity is concentration dependent (Fig. 2F). It is known that the N-terminus of the p14arf mouse homologue p19arf interacts with the N-terminal domain of NPM1 (residues 16–123; hereby NPM1-Nter) [21] and that NPM1-Nter displays molecular chaperone activity on several proteins [25]. Therefore, we checked whether NPM1-Nter exerts chaperone activity on p14arf. This is indeed the case, as shown in Fig. 2G, with a significant decrease in p14arf (0.1 μM) turbidity at 43 °C when NPM1-Nter is present at 3-fold excess and a complete loss of aggregation with 5-fold excess.

Structural analysis of the p14arf interaction with NPM1-Nter

We then aimed at characterizing the interaction between p14arf and NPM1-Nter at the residue level by NMR spectroscopy. Given the high tendency of p14arf to aggregate and precipitate in the absence of urea, we sought to perform also these experiments in 20 mM phosphate buffer pH 7.1 containing 4 M urea. Therefore, prior to NMR characterization, we checked whether NPM1-Nter is still folded in this condition. Figure 3A shows static CD spectra of the protein, collected at urea concentrations ranging from 0 to 8 M. These data indicate that NPM1-Nter is folded up to 7 M urea while it starts denaturing only at 8 M urea. To assess whether 4 M urea influenced the oligomerization state of NPM1-Nter, we also performed size exclusion chromatography coupled to multiangle light scattering (SEC-MALS) experiments in 20 mM phosphate buffer pH 7.1 with and without 4 M urea. In the absence of urea (Fig. 3B), NPM1-Nter elutes as a single peak of 72 kDa MW, which can be attributed to a pentamer (MW of the monomer = 14 kDa). In the presence of 4 M urea, NPM1-Nter still elutes as a single peak with a MW of 56 kDa (Fig. 3C). The lower MW calculated in 4 M urea might indicate a different quaternary structure, i.e. a tetramer. This is, however, unlikely, given the hydrophobicity of the contact surface at the monomer–monomer interface, and has never been observed [21]. More likely, in the presence of 4 M urea, the monomer–pentamer equilibrium is slightly shifted toward the monomer, even though the pentamer is still the predominant species.

Titration of ^{15}N-labeled p14arf with unlabeled NPM1-Nter (up to 10 equivalents of NPM1-Nter monomer), in 20 mM phosphate buffer pH 7.1 and 4 M urea, resulted in several p14arf crosspeaks decreasing in intensity and accompanied by minor but measurable chemical shift perturbations in the region of p14arf detectable by NMR (Fig. 4A,B). An excess of NPM1-Nter was required to observe this effect, indicating the occurrence of weak interactions between the two proteins. This behavior was confirmed by comparing the ^{15}N relaxation properties of ^{15}N-p14arf in complex with NPM1-Nter in a 1 : 10 ratio with those of the free protein (Fig. 5). Notably, the chemical shift variations (Fig. 5A), the signal intensity ratios (Fig. 5B) and the ^{15}N relaxation data (Fig. 5C–E) indicate that NPM1-Nter interacts with a region of p14arf roughly comprised between amino acids 84 and 103. In this

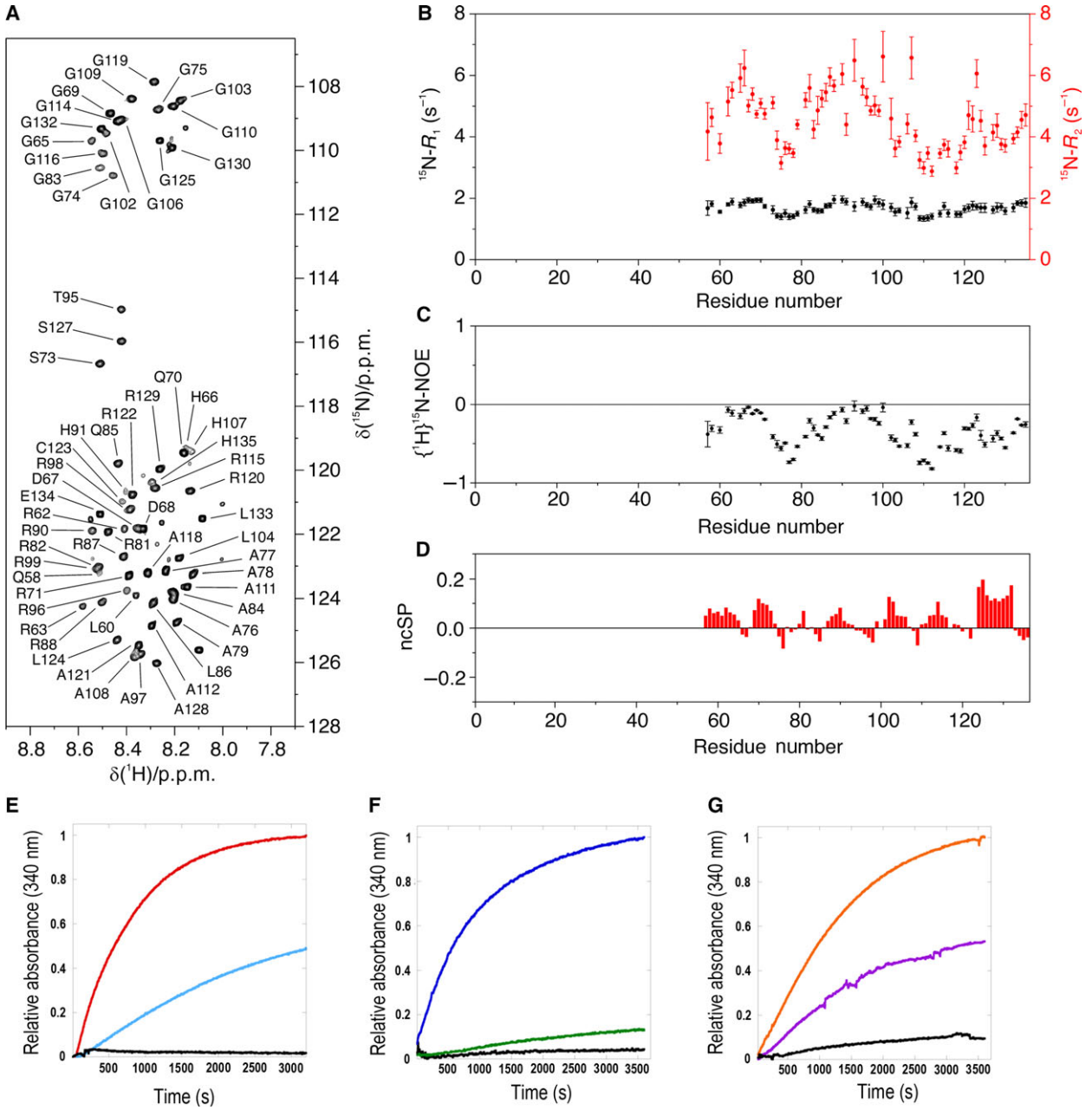

Fig. 2. NMR analysis of p14arf structure and aggregation. (A) Backbone resonance assignment of p14arf overlaid to the ^{1}H–^{15}N HSQC spectrum of ^{15}N-p14arf in 4 M urea at 298 K. (B) Plot of the longitudinal (R_1) and transverse (R_2) ^{15}N-amide relaxation of the assigned residues; standard errors derived from the fitting are reported. (C) Plot of the ^{15}N-NOE of the assigned residues; errors were calculated from the standard deviation of the spectral noise divided by signal intensity. (D) ncSP of p14arf calculated from the ^{15}N, $^{13}C'$, $^{13}C\alpha$ and $^{13}C\beta$ secondary chemical shifts measured at 288 K; positive and negative values indicate propensities for a-helix and b-strand, respectively. (E) Turbidity assay of p14arf (0.3 μM) at 20 °C (black), 43 °C (cyan) and 60 °C (red). (F) Turbidity assay, at 37 °C of p14arf at 0.1 μM (black), 0.3 μM (green) and 0.7 μM (blue). (G) Turbidity assay of p14arf (0.1 μM) alone (orange) or in the presence of NPM1-Nter 0.3 μM (magenta) or 0.5 μM (black), all at 43 °C.

region, the ^{15}N transverse relaxation rates (R_2) increase markedly upon interaction with NPM1-Nter, whereas the longitudinal relaxation rates (R_1) remain unchanged, indicating that the p14arf-NPM1-Nter complex is in the intermediate-fast exchange regime with the free proteins.

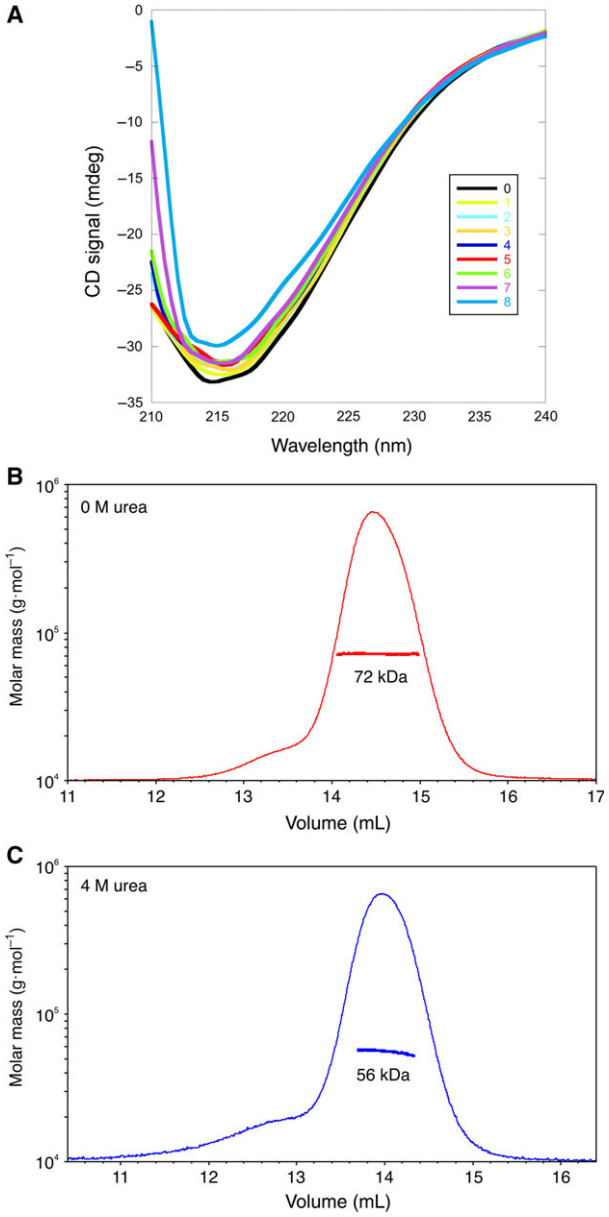

Fig. 3. Analysis of NPM1-Nter in the presence of urea. (A) Static CD spectra of NPM1-Nter (40 μM) were collected in 20 mM phosphate buffer pH 7.1 plus urea concentrations ranging from 0 to 8 M at 1 M interval. All spectra shown are the average of 10 scans. (B) SEC-MALS analysis of NPM1-Nter in buffer containing 0 M urea (red trace). (C) SEC-MALS analysis of NPM1-Nter in buffer containing 4 M urea (blue trace). Molecular masses calculated from the multiangle detector (squares) are also shown.

We also performed the reverse titration in the same mildly denaturing conditions. However, when ^{15}N-NPM1-Nter was titrated with unlabeled p14arf, the NMR signals of ^{15}N-NPM1-Nter almost disappeared after addition of as low as 0.1 equivalents of p14arf

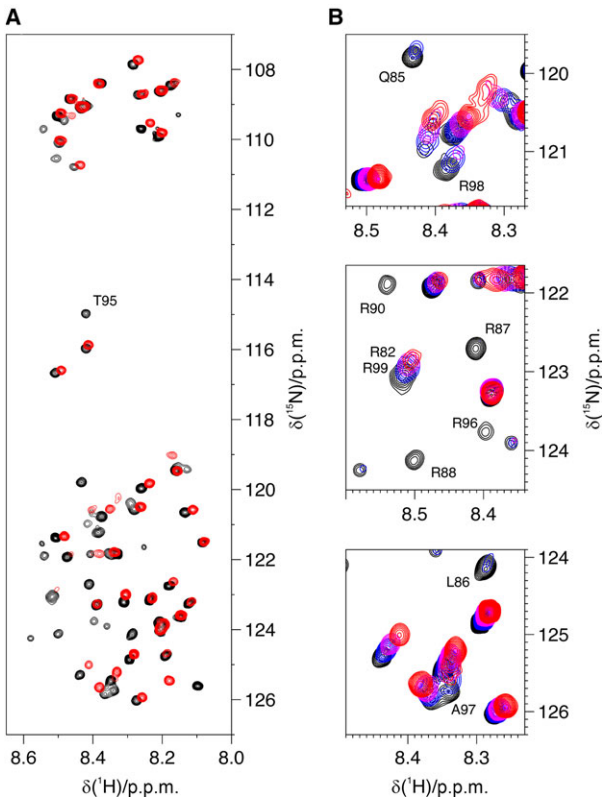

Fig. 4. Interaction of ^{15}N-p14arf with NPM1-Nter. (A) ^{1}H–^{15}N SOFAST-HMQC spectrum of ^{15}N- p14arf acquired at 298 K in 4M urea, in absence (black) and in presence (red) of 10 eq. of NPM1-Nter. (B) Changes in chemical shift and signal intensity of ^{15}N-p14arf signals upon titration with NPM1-Nter. The overlaid spectra correspond to 0 eq. (black), 1 eq. (blue), 2 eq. (magenta) and 10 eq. (red) of NPM1-Nter.

per NPM1-Nter monomer, likely due to the formation of high molecular weight species at substoichiometric amounts of p14arf.

Analysis of the interaction between NPM1-Nter and the p14arf (84–103) peptide

The finding that an additional, and previously unreported, region of p14arf interacts with NPM1-Nter prompted us to further investigation. NPM1 has been recently reported to recognize arginine-rich motives in its protein partners, which often correspond to their NoLS [26,27]. Therefore, we checked whether p14arf possesses a NoLS as predicted by the NoD algorithm, which scans a protein sequence in search of local enrichments of positive charges [28]. Interestingly this analysis retrieved a putative NoLS in the same region (84–103) that we identified in p14arf through NMR analysis (Fig. 6A,B). Moreover, this region is only

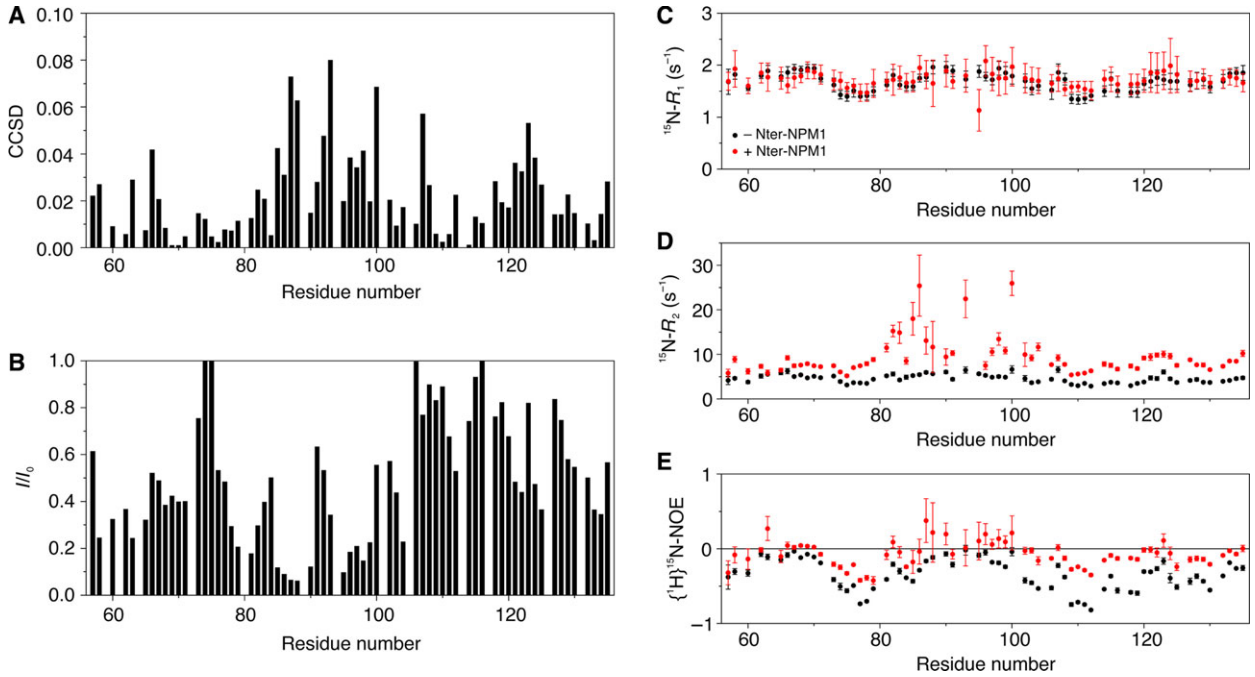

Fig. 5. NMR characterization of p14arf:NPM1-Nter (1 : 10). (A) CCSD and (B) signal intensity ratio calculated for each assigned residue between free p14arf and p14arf:NPM1-Nter (1 : 10) complex. (C,D) Longitudinal (C) and transverse (D) relaxation of free p14arf (black) and p14arf in complex with NPM1-Nter (red); standard errors derived from the fitting are reported. (E) ^{15}N-NOE of free p14arf (black) and p14arf in complex with NPM1-NPM1 (red); errors were calculated from the standard deviation of the spectral noise divided by signal intensity.

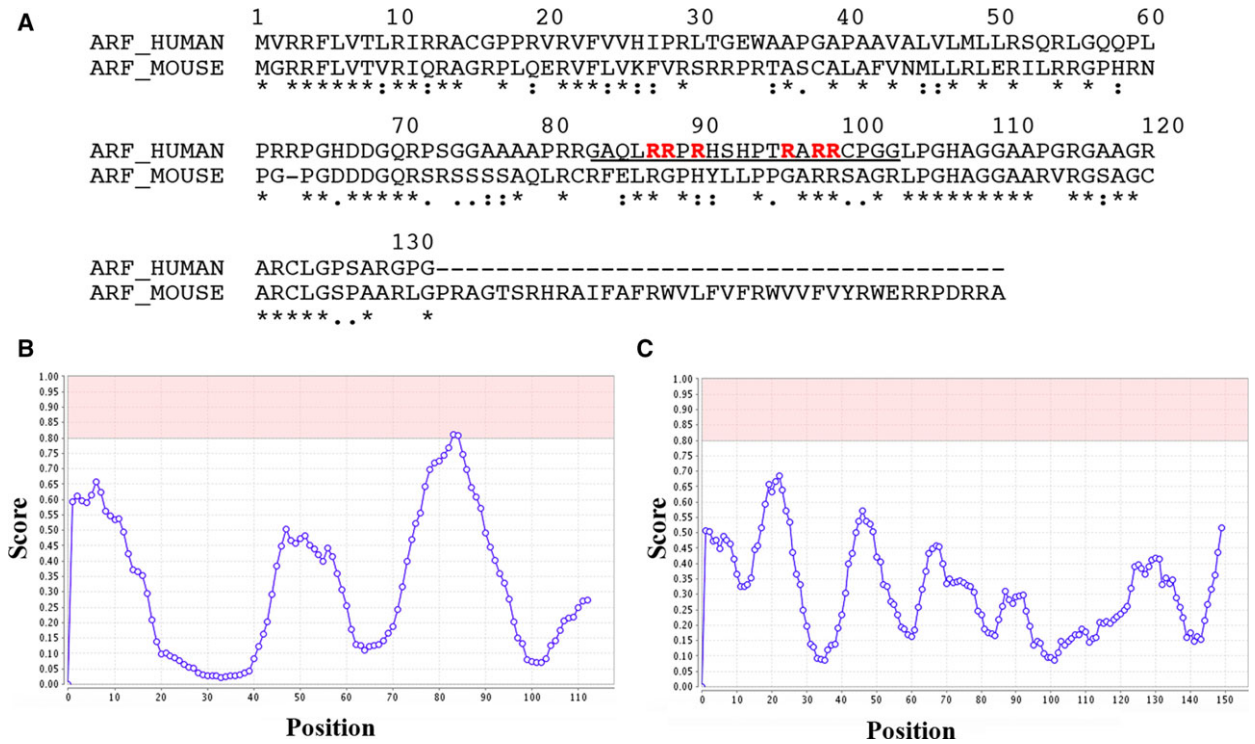

Fig. 6. Prediction of p14arf and p19arf NoLS. The human p14arf and mouse p19arf sequences (aligned in panel A) were run against the NoD server and the relative scores are shown on panel B for p14arf and on panel C for p19arf. The predicted NoLS of p14arf is underlined in the sequence alignment; in p19arf this motif is only partially conserved and not predicted to be a NoLS (panel A).

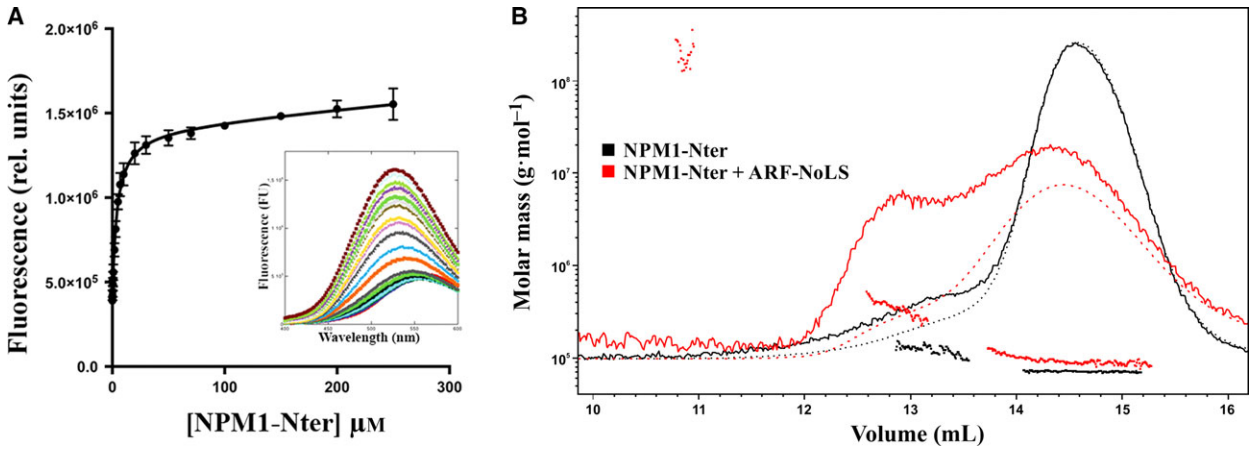

Fig. 7. Analysis of the NPM1-Nter:p14arf-NoLS complex. (A) Equilibrium fluorescence titration of a dansylated p14arf-NoLS peptide (5 μM) with increasing amounts of NPM1-Nter. Fluorescence intensities at 528 nm were fitted with Eqn (1). Data are represented as mean ± SD (n = 3). Full spectra from a representative titration are reported in the inset. (B) SEC-MALS analysis of free NPM1-Nter (black) and NPM1-Nter incubated overnight with two equivalents of p14arf-NoLS (red). Refractive index (dotted line), scattering (line) and calculated molecular mass (squares) are shown.

partially conserved and not predicted to be a NoLS in mouse p19arf (Fig. 6A–C).

To gain further insight on this interaction, we performed equilibrium fluorescence titrations of a peptide comprising residues 84–103 of p14arf (p14arf-NoLS), tagged with a dansyl group at its N terminus, with NPM1-Nter (Fig. 7A). This analysis confirmed binding and the data, fitted with Eqn (1) (see Materials and methods), yielded a dissociation constant for the complex of K_D = 3.9 ± 0.3 μM (Table 1).

We further investigated the interaction of p14arf-NoLS with NPM1-Nter by NMR. Differently from full-length p14arf, p14arf-NoLS is highly soluble in aqueous buffer and urea was not required. However, addition of already one equivalent of p14arf-NoLS to ^{15}N-NPM1-Nter caused the complete loss of protein signals suggesting, once again, the formation of high molecular weight species in slow exchange with the free protein.

Table 1. p14arf-NoLS and selected mutants interaction with NPM1-Nter.

Peptide name	Sequence	K_D (μM)
P14arf-NoLS	^{84}AQLRRPRHSHPTRARRCPGG^{103}	3.9 ± 0.3
Cluster1	^{84}AQL**AA**P**A**HSHPTRARRCPGG^{103}	154 ± 30
Cluster2	^{84}AQLRRPRHSHPT**AA**R**AA**CPGG^{103}	76 ± 3
R87C	^{84}AQL**C**RPRHSHPTRARRCPGG^{103}	5.8 ± 0.7
R88Q	^{84}AQLR**Q**PRHSHPTRARRCPGG^{103}	9 ± 1
R90H	^{84}AQLRRP**H**HSHPTRARRCPGG^{103}	6.2 ± 0.6
R98L	^{84}AQLRRPRHSHPTRA**L**RCPGG^{103}	6.1 ± 0.6
R99S	^{84}AQLRRPRHSHPTRAR**S**CPGG^{103}	6.0 ± 0.3

Bold indicates mutated residues.

This hypothesis was confirmed by SEC-MALS experiments performed in 20 mM phosphate buffer pH 7.1 (Fig. 7B). A broad peak is observed in the chromatogram of a 1 : 2 mixture of NPM1-Nter:p14arf-NoLS, at a smaller elution volume than free pentameric NPM1-Nter. This peak has a calculated MW of 200–500 kDa, consistent with the formation of large aggregates, while the MW calculated on the peak of pentameric NPM1-Nter increases from 72 kDa to 95 kDa, suggesting that a complex could be formed between a NPM1 pentamer and several p14arf-NoLS peptides. Given the high positive net charge of p14arf-NoLS, we assumed that the nature of its interaction with NPM1-Nter would be mainly electrostatic. Therefore, we repeated the NMR titration experiment under high salt conditions to decrease the electrostatic contribution. Indeed, in 20 mM phosphate buffer pH 7.1 plus 500 mM NaCl, the interaction was sufficiently weakened to allow the NMR signals of NPM1-Nter to be observed upon titration with up to 10 equivalents of p14arf-NoLS (Fig. 8A). Under these conditions, small chemical shift variations were observed, together with an increase in line-width, indicative of an exchange between the free protein and the aggregated, high molecular weight complex, which could be mapped to the NPM1-Nter structure (Fig. 8B). From the resulting data, several residues were identified that are putatively involved in the interaction with the peptide. Among them, the largest chemical shift variations were observed for residues 29–32, 37–41, 67–68 and

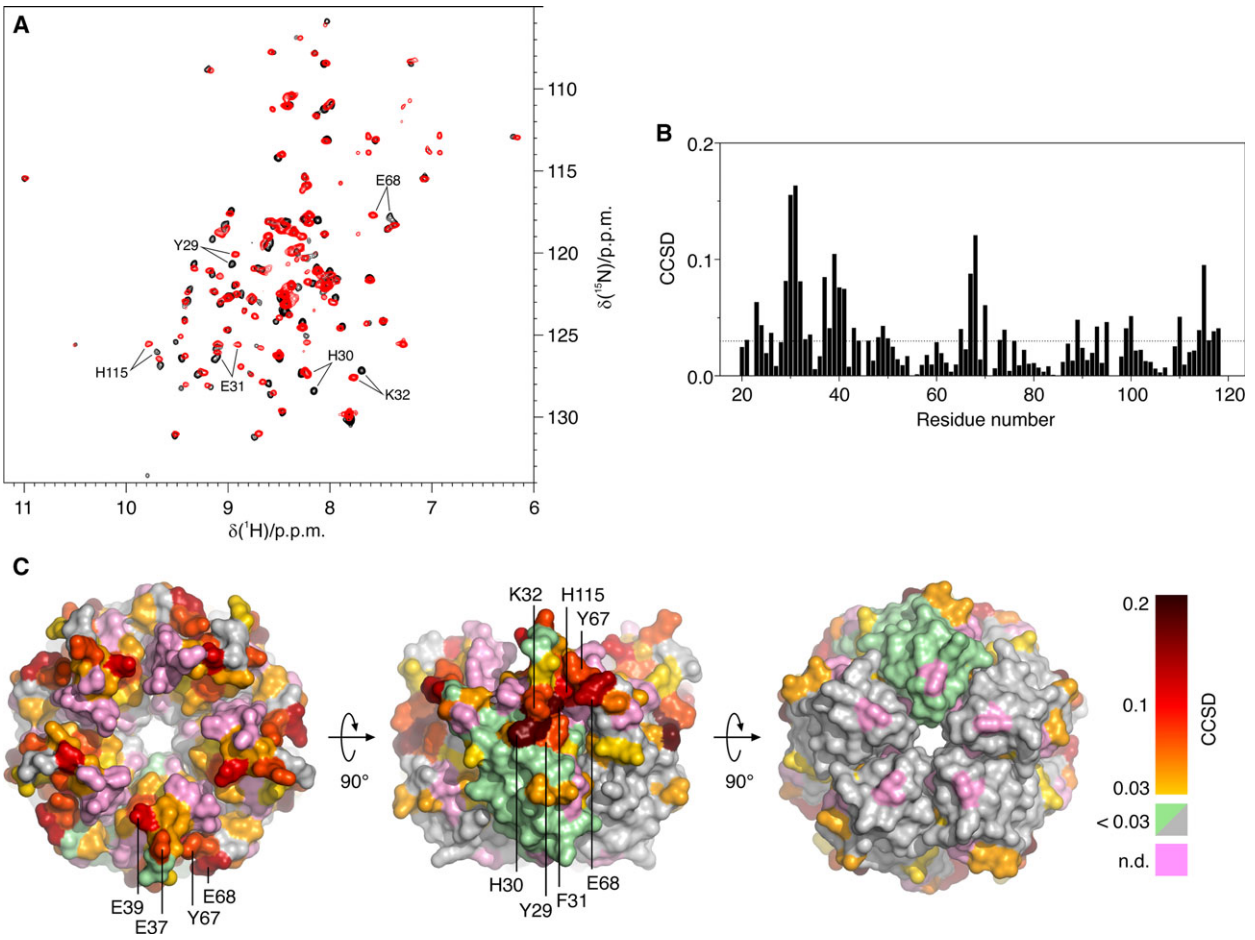

Fig. 8. NMR analysis of the interaction between ^{15}N-NPM1-Nter and p14arf-NoLS. (A) ^{1}H–^{15}N TROSY spectrum of ^{15}N-NPM1-Nter acquired at 310 K in the absence (black) and in the presence (red) of 10 eq. of p14ARF-NoLS peptide. (B) CCSD plot calculated between free NPM1-Nter and NPM1-Nter:p14ARF-NoLS (1 : 10) complex; CCSD standard deviation (SD = 0.03) is shown as a dotted line. (C) The surface of the NPM1-Nter pentameric structure (PDB ID: 4N8M) is represented with residues significantly perturbed by the interaction with p14arf-NoLS color coded based on their CCSD values (yellow < red < black); unassigned residues are shown in pink; one monomer is shown in light green.

115 of NPM1-Nter (Fig 8A,B). Collectively, these residues identify an extended region on the external surface of each NPM1-Nter monomer, which is implicated in p14arf-NoLS binding (Fig. 8C).

Mutational analysis

The p14arf-NoLS peptide sequence is ^{84}AQL**RR**P**R**HSHPT**RARR**CPGG^{103} and contains two clusters of three arginines each. We next wanted to check whether both clusters are implicated in binding NPM1-Nter. To this purpose we used two modified dansylated peptides and measured their interaction with NPM1-Nter through equilibrium fluorescence spectroscopy. The concomitant mutation into alanine of Arg87, Arg88 and Arg90 in Cluster1 peptide (Table 1) had a significant effect on the affinity of p14arf-NoLS for NPM1-Nter, yielding a K_D for the complex 40-fold higher than with wild-type. Likewise, the concomitant mutation of Arg96, Arg98 and Arg99 (Cluster2 peptide) led to an almost 20-fold increase in the K_D, showing that also this cluster of arginine residues is important for NPM1-Nter recognition (Table 1).

This NoLS region of p14arf is frequently deleted, or subject to missense mutations in multiple cancers [4,29]. Most of the identified missense mutations involve the arginine residues of the NoLS. Among them we tested the Arg87Cys, Arg88Gln and Arg90His mutations in the first cluster and the Arg98Leu and Arg99Ser mutations in the second cluster (Table 1). Mutation of Arg88 into glutamine led to an increase

in the dissociation constant of 2,3-fold, while all other mutations resulted in a K_D 1,5-fold higher than wild-type (Table 1).

Discussion

P14arf is a critical player of the most important tumor-suppressive mechanism in our cells, i.e. the p14arf-HDM2-p53 axis [9]. Therefore, it is not surprising that not only p53 but also p14arf is the frequent target of deletions or mutations in several cancers [4,29]. In AML with NPM1 mutations, both p14arf and p53 are wild-type but, nevertheless, their tumor-suppressive functions are strongly impaired by the aberrant p14arf translocation in the cytosol due to mutated NPM1 [18,30,31]. Unveiling the details of the p14arf-NPM1 interaction may thus have a therapeutic value because a drug capable of interfering with this association may rescue p14arf levels in the leukemic blasts and activate p53-mediated apoptosis or cell-cycle arrest [20].

Other groups had already shown that the N-terminal segment of the p14arf mouse homologue p19arf interacts with NPM1-Nter [32,33]. Moreover, a structural investigation of mouse NPM1-Nter in complex with a peptide comprising the first six residues of p19arf (see Fig. 6) has been recently published [21].

Starting from these premises, we further investigated the determinants of this complex. First, we analyzed the structural properties of full-length p14arf in solution. We observed the formation of high molecular weight homo-oligomers of p14arf, likely mediated by its N-terminal end. Interestingly the N-terminal half of mouse p19arf had already been shown to form fibril-like heteropolymers with its cognate peptide from HDM2 [34]. PSIPRED predictions indicated a propensity for p14arf to form two β-strands in the 1–30 region (see Fig. 1), which may mediate the formation of homopolymers. We also showed that p14arf aggregates form in a temperature- and concentration-dependent fashion, and that NPM1-Nter acts as a chaperone on p14arf, similarly to what already established with other proteins [25]. Therefore, not only NPM1 is responsible for p14arf nucleolar localization [18] but may also prevent its aggregation within the cell. However, when analyzing their interaction, we observed a tendency of the two proteins to form soluble, high molecular weight complexes even in moderately denaturing conditions. Interestingly, within these complexes, we could identify a previously unknown region of p14arf that interacts with NPM1-Nter, comprised between residues 84–103. This finding captured our attention for several reasons. This region is enriched in arginine residues and it has been recently shown that arginine-rich motives, isolated from proteins such as rpL5, are recognized by NPM1-Nter with the formation of large assemblies resembling liquid-like droplets phase separated from the solvent [26]. Furthermore, the very same region is predicted to be the p14arf NoLS and previous data suggested that it is sufficient to partially drive the nucleolar localization of the protein [35]. As it was previously thought that only the N-terminal region of p14arf mediated the interaction with NPM1 [32,33], our data add a new layer of complexity in the formation of this complex. Interestingly, as shown in Fig. 6, the p14arf-NoLS region of p14arf we identified here is only partially conserved in mouse p19arf. This raises the possibility that, in mice, the N-terminal region of p19arf may suffice for the formation of the assemblies with NPM1. Alternatively, it may also be hypothesized that other regions of p19arf may play the same role as p14arf-NoLS in p14arf. In particular, p19arf is characterized by a 40-residue-long C-terminal extension with respect to p14arf. At the end of this additional region a cluster of five arginines within 10 residues is present (see Fig. 6).

Previous analysis conducted with the mouse p19arf (1–6) N-terminal peptide had identified three acidic residues, namely, Asp36, Glu39 and Glu93 that are conserved in human NPM1 and are implicated in the interaction [21]. Our next step was to verify whether the same region of NPM1-Nter is also implicated in the recognition of the p14arf 84–103 region. We showed through fluorescence spectroscopy that the peptide p14arf-NoLS, which encompasses residues 84–103 of p14arf, is able to bind NPM1-Nter with a dissociation constant in the low micromolar range. Then, through the NMR analysis of the complex in high salt conditions, we could identify several residues in NPM1-Nter that show chemical shift variations upon binding. Taken together, these residues identify the p14arf-NoLS interacting region on the external surface of the NPM1-Nter pentamer and comprising residues Tyr29, Phe31, Lys32, Glu37, Glu39, Tyr67, Glu68 and His115 (see Fig. 8). This region comprises residue Glu39 and therefore partially overlaps with the one recognizing the p19arf(1–6) peptide, but it is overall more extended. This may be due to the larger size of the p14arf-NoLS peptide (20 residues), which allowed the identification of additional interacting residues in NPM1-Nter.

The p14arf-NoLS peptide contains two stretches of three arginine residues each, between residues 87–90 and 96–99, respectively, whose role in the interaction has been analyzed. Analysis of the Cluster1 and Cluster2 peptides binding to NPM1-Nter (see Table 1)

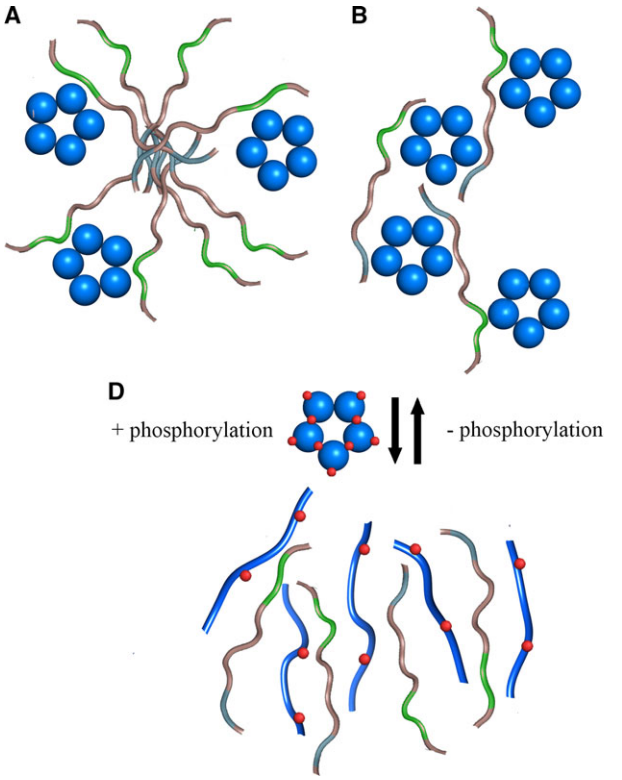

Fig. 9. Schematic drawing of p14arf-NPM1-Nter heteropolymerization. (A) p14arf may form homo-oligomers with its N-terminal end, while interacting with different NPM1-Nter pentamers with its central NoLS region. (B) Both the N-terminal end and the central NoLS regions of p14arf may engage different NPM1-Nter pentamers. (C) The NoLS region of p14arf may engage two different NPM1-Nter pentamers at the same time with its two arginine clusters, leaving the N-terminal ends free to interact with other NPM1-Nter pentamers. (D) Upon sequential phosphorylation of different exposed and buried Ser/Thr sites played by several kinases, NPM1-Nter monomerizes and unfolds thus releasing active p14arf in the nucleoplasm. NPM1-Nter monomers are represented as blue spheres or ribbons (in panel D), while p14arf is represented as a ribbon with the N-terminal region colored in cyan and the central NoLS region in green. Red dots represent phosphorylation sites in NPM1-Nter.

indicated that both of them are implicated in the interaction, with a slightly major contribution played by Cluster1 with respect to Cluster2.

Overall, the experiments we have reported here suggest that the formation of high molecular weight assemblies between NPM1-Nter and p14arf may be more complex than previously thought, and may proceed through several pathways, that may also take place in parallel. Indeed, our data suggest at least three possible scenarios (Fig. 9). First, p14arf may form homo-oligomers, through its N-terminal end, while interacting also with NPM1-Nter, through its NoLS region (Fig. 9A). Second, the same p14arf molecule may contact two NPM1-Nter pentamers through its N-terminal and NoLS regions, respectively (Fig. 9B). Finally, as suggested by our SEC-MALS experiment (see Fig. 7B) and mutational data, the NoLS region of p14arf may engage at the same time two NPM1-Nter pentamers with its two arginine clusters, leaving the N-terminal end free to interact with itself or with another NPM1-Nter pentamer (Fig. 9C). Furthermore, it should be noted that full-length NPM1 also contains a central unstructured domain enriched with negatively charged residues, which may themselves interact with p14arf. Therefore, the interaction between the two proteins in the physiological context may be even more intricate.

Once these assemblies are formed within nucleoli, p14arf is sequestered by NPM1 in this compartment in a dormant state. Therefore, to exert its tumor-suppressive functions in the nucleoplasm, p14arf needs to be 'liberated' by its interaction with NPM1-Nter. It is well known that p14arf is upregulated in response to several oncogenic signals [7] and increased levels of p14arf may unbalance the NPM1-p14arf assemblies and favor the release of p14arf from nucleoli. However, an important regulatory role played by NPM1 may also be envisaged. Indeed, NPM1-Nter is phosphorylated at various sites by different kinases, in response to a variety of stress signals [10,11,36]. Recent data suggested that the sequential phosphorylation of solvent exposed and buried serine and threonine residues within NPM1-Nter results in a pentamer-to-monomer transition which is coupled to the complete unfolding of the domain [21]. Whenever this happens, the large molecular weight assemblies with p14arf would likely be dissolved thus releasing p14arf in the nucleoplasm (Fig. 9D). Therefore, NPM1 may act as a switchable guardian of p14arf activity under stress conditions. As NPM1-Nter recognizes several proteins through clustered arginine-rich motives, this model may be also relevant for the interaction of NPM1 with different partners.

The p14arf 84–103 NoLS region is also the subject of mutations reported in several cancers, which may introduce stop codons or substitute single residues [4,29]. Notably, five of six arginine residues in the region are mutated in cancers and we tested the interaction of the corresponding p14arf-NoLS variants with NPM1-Nter (see Table 1) [29]. Our data argue against a major effect of these mutations in disrupting the interaction with NPM1-Nter, with increases in the dissociation constant comprised between 1.5- and 2.3-fold. However, an effect played by the mutations on the interaction with full-length NPM1, through its central domain, cannot be excluded at present. Furthermore, even when considering NPM1-Nter only, a modest perturbation *in vitro* may still have an effect *in vivo*. For instance, it has been shown that the Arg88Gln mutation, which doubles the p14arf-NoLS-NPM1-Nter dissociation constant (see Table 1), caused an ample diffusion of the protein from the nucleoli to the nucleoplasm and the cytoplasm when p14arf was overexpressed in U2-OS cells [29]. Notably, the very same mutations were also shown to be detrimental for the formation of the complex between p14arf and the mitochondrial protein p32, thus impairing the p53-dependent mitochondrial activation of apoptosis played by p14arf [37]. Our findings therefore indicate the need for further *in vivo* investigation of the effect of p14arf mutations on the interaction with NPM1.

In conclusion, we have provided here novel insight into the NPM1–p14arf interaction. We have identified a previously unknown region of p14arf that is recognized by NPM1-Nter and identified residues that are implicated in binding. These data may facilitate the design of peptidomimetic molecules or small chemicals that interfere with this interaction, to be tested for the treatment of AML and possibly other cancers.

Materials and methods

Protein expression and purification

Human NPM1-Nter (residues 16–123) was expressed and purified as follows. A codon-optimized coding sequence was obtained through gene synthesis (GeneArt, Regensburg, Germany) and subcloned into expression vector pET28a(+) under restriction sites NdeI and BamHI. The resulting plasmid was transformed into *Escherichia coli* strain BL21 (DE3). Cells were grown in LB medium supplemented with kanamycin at 37 °C to $A_{600} \sim 0.5$, at this point 1 mM IPTG was added to induce expression. Cells were further grown overnight at 20 °C. For isotope enrichment, cells were grown in a minimal medium supplemented with ($^{15}NH_4SO_4$) and/or [^{13}C]-glucose (Cambridge Isotope Laboratories Inc., Tewksbury, MA, USA), and induced in the same way. After centrifugation, cells were resuspended in lysis buffer (20 mM Hepes, pH 7.1, 20 mM imidazole), plus 5 mM $MgCl_2$, 2 $\mu g \cdot mL^{-1}$ DNAse (Roche, Basel, Switzerland), Protease Inhibitor Cocktail Tablet (Roche) and sonicated. Nucleic acids were digested for 30′ at 37 °C with DNAse I. NPM1-Nter is expressed with a histidine-tag at its N -terminus and was purified by affinity chromatography (HisTrap FF; GE Healthcare, Chicago, IL, USA) with a linear gradient of lysis buffer plus imidazole (from 20 mM to 1 M) on a AKTA-Prime FPLC apparatus, followed by anion exchange chromatography (Q-Sepharose FF; GE Healthcare) eluted with a NaCl gradient. Fractions containing the protein, as shown by SDS/PAGE, were collected, buffer exchanged and concentrated in Hepes 20 mM pH 7.1, using Amicon® Ultra-15 Centricons with a 3 kDa cutoff (Merck Millipore, Darmstadt, Germany), and stored at −20 °C.

The coding sequence of human full-length p14arf was obtained through gene synthesis and cloned into a pET28a(+) expression vector under restriction sites NcoI and XhoI. *Escherichia coli* BLR (DE3) cells (Novagen, Madison, WI, USA), transformed with the expression vector, were grown to $A_{600} \sim 0.5$ in LB medium supplemented with kanamycin at 37 °C. Expression was induced by addition of 0.5 mM IPTG and cells were further grown at 20 °C for 16 h. For isotope enrichment, cells were grown in a minimal medium supplemented with ($^{15}NH_4SO_4$) and/or [^{13}C]-glucose (Cambridge Isotope Labelling Inc.), and induced in the same way. After induction, cells were collected by centrifugation, resuspended in lysis buffer (50 mM Hepes pH 7.1, 150 mM NaCl, 6 M GndHCl and 1 mM DTT) plus Protease Inhibitor Cocktail Tablet (Roche) and sonicated. Protein was purified by affinity chromatography (HisTrap FF; GE Healthcare) using a step elution with Buffer A (50 mM Hepes pH 7.1, 150 mM NaCl, 8 M urea and 1 mM DTT) plus Imidazole (15 mM, 300 mM, 500 mM and 1 M). Fractions containing the protein, as showed by SDS/PAGE, were collected, dialyzed against the buffer 20 mM sodium phosphate, pH 7.1, 4 M urea and 1 mM DTT, and concentrated using Amicon Ultra-15 centricons with a 10 kDa cutoff (Merck Millipore). The protein was stored at −20 °C. The p14arf NoLS peptide and variants (sequences reported in Table 1) were synthesized and dansylated at their N terminus by JPT (Berlin, Germany).

Aggregation and chaperone activity

The aggregation propensity of p14arf was monitored by measuring the zero-angle light scattering with a UV-visible spectrophotometer V650 (Jasco Inc., Easton, MD, USA). Ice-cold p14arf was diluted in Hepes 50 mM pH 7.1 and protein aggregation was monitored over time. For temperature-dependence experiments, protein concentration was set to

0.3 μM and aggregation was monitored at 20, 43 and 60 °C. For protein concentration dependence, temperature was set to 37 °C and aggregation was monitored with p14arf concentration set to 0.1, 0.3 and 0.7 μM. To assess the chaperone activity of NPM1-Nter, temperature was set to 43 °C and p14arf (0.1 μM) aggregation was followed alone and in the presence of three or five excesses of NPM1-Nter.

CD

All CD experiments were performed using a JASCO J710 instrument (Jasco Inc.) equipped with a Peltier apparatus for temperature control.

Spectra were collected using a quartz cell with 1 mm optical path length (Hellma, Plainview, NY, USA) and a scanning speed of 100 nm·min^{-1}. Static spectra of p14arf (15 μM) in 20 mM phosphate buffer pH 7.1, in the absence or presence of trifluoroethanol, are the average of three scans. Thermal denaturation experiment on p14arf sample was performed by monitoring the variation in CD signal at 222 nm with temperature progressively increasing, in 1 °C·min^{-1} steps, from 20 to 90 °C. Static spectra of NPM1-Nter (40 μM) in 20 mM phosphate buffer pH 7.1 plus urea from 0 to 8 M are the average of 10 scans. Data were represented using KALEIDAGRAPH software (Synergy Software, Reading, PA, USA).

Equilibrium binding assays

The interactions between NPM1-Nter and the p14arf-NoLS and variant peptides were monitored through equilibrium binding experiments. Titrations were performed at 25 °C with a FluoroMax-4 spectrofluorometer (Jobin Yvon, Edison, NY, USA) equipped with a water bath apparatus. Experiments were all performed in sodium phosphate buffer 20 mM pH 7.1. Excitation wavelength was 330 nm while emission spectra were recorded in the 350–650 range. Titrations were performed keeping fixed at 5 μM the concentration of the dansylated peptide (p14arf-NoLS and mutants) and varying NPM1-Nter concentration (from 0 to 200/400 μM). At least three independent titrations were performed for each peptide and data were globally fitted, within the GRAPHPAD Prism software (GraphPad Software Inc., La Jolla, CA, USA), using Eqn (1):

$$F = \left\{ \left[\frac{([A]_0 + K_D + n)}{2} - \sqrt{\frac{([A]_0 + K_D + n)^2}{4} - [A]_0 n} \right] B + C \right\} k \quad (1)$$

where F is the observed fluorescence, n and $[A]_0$ refer to the concentration of nonvaried and varied species, respectively, and K_D is the equilibrium dissociation constant. B and C are constants that take into account the total fluorescence change and fluorescence at $[A]_0 = 0$, respectively, whereas k describes the slope of the curve at high protein concentration.

NMR experiments

Backbone sequential assignment of p14arf

NMR experiments for the sequence-specific resonance assignment of full-length p14arf were acquired on a sample containing 250 μM [U-^{13}C,^{15}N]-labeled p14ARF in 20 mM phosphate buffer, 4 M urea, pH 7.1. ^{1}H-detected 2D ^{1}H–^{15}N SOFAST-HMQC and triple resonance experiments 3D HNCO, 3D HN(CA)CO, 3D HNCA, 3D HN(CO)CA, 3D HNCACB and 3D HN(CO)CACB were acquired on a 950 MHz Bruker Avance spectrometer equipped with a TCI CryoProbe. ^{13}C-detected experiments 2D C-CON, 2D (H_N)-CON, 3D (H)CBCACON and 3D (H)CBCANCO were acquired on a 700 MHz spectrometer equipped with a TXO CryoProbe optimized for ^{13}C direct detection. All the data were acquired at 288 K to maximize the sample stability and the intensity of the amide signals. The NMR spectra collected were processed with Topspin NMR data processing software and analyzed with CARA. The resonance assignment obtained at 288 K was transferred to the ^{1}H–^{15}N NMR spectra of [U-^{15}N]-labeled p14ARF recorded at 298 K, by collecting a series of spectra at increasing temperatures.

Interaction between full-length p14arf and NPM1-Nter

A titration experiment between [U-^{15}N]-labeled p14arf and unlabeled NPM1-Nter was performed in 20 mM phosphate buffer, 4 M urea, pH 7.1, at 298 K on a 950 MHz spectrometer. Unlabeled NPM1-Nter was added to p14arf (500 μM) at increasing concentrations, up to 10 equivalents of NPM1-Nter monomer. The reverse titration experiment between [U-^{15}N]-labeled NPM1-Nter and unlabeled p14arf was performed at 298 K on a 950 MHz spectrometer, in the same buffer as the previous experiment. Unlabeled p14arf was added to NPM1-Nter (150 μM) at increasing concentrations up to 2.9 equivalents (referred to the NPM1-Nter monomer). Spectral changes were monitored by acquiring ^{1}H–^{15}N SOFAST-HMQC spectra after each addition. Changes in chemical shift and signal intensity were obtained with CARA. Signal intensity ratios (I/I_0) were calculated dividing the crosspeak intensities in the final spectrum (corrected for sample dilution) by those of the initial spectrum. Combined chemical shift differences (CCSD) were calculated for each amide crosspeak with the following formula:

$$\mathrm{CCSD} = \sqrt{\frac{1}{2}(\Delta\delta\ ^{1}\mathrm{H})^2 + \frac{1}{2}(\Delta\delta\ ^{15}\mathrm{N}/5)^2}$$

Neighbor-corrected structural propensity (ncSP) of p14arf was calculated from the ^{15}N, $^{13}C'$, $^{13}C\alpha$ and $^{13}C\beta$ secondary chemical shifts measured at 288 K using the ncSPC web tool (http://nmr.chem.rug.nl/ncSPC) and the 'Tamiola Acar and Mulder (2010)' random-coil chemical shift library [38].

Heteronuclear relaxation and NOE experiments

^{15}N-R_1, R_2 relaxation and $\{^1H\}^{15}N$-NOE experiments on free [U-^{15}N]-labeled p14arf (500 μM) and on [U-^{15}N]-labeled p14ARF–NPM1-Nter (1 : 10) complex (300 μM p14arf) in 20 mM phosphate buffer, 4 M urea, pH 7.1, were acquired on a 500 MHz spectrometer equipped with a TCI CryoProbe at 298 K. The ^{15}N-R_1, R_2 relaxation data and standard errors were obtained by integrating the signal intensity at increasing evolution times for each assigned residue and by fitting with monoexponential decays in ORIGINPRO (OriginLab Corporation, Northampton, MA, USA).

Interaction between NPM1-Nter and P14arf-NoLS

Titration experiments of [U-^{15}N]-labeled NPM1-Nter with unlabeled p14arf-NoLS peptide were performed in 20 mM phosphate buffer, pH 7.1, at 310 K on a 900 MHz Bruker Avance spectrometer equipped with a TCI CryoProbe. Several titrations were performed on samples of 200 μM [U-^{15}N]-labeled NPM1-Nter in buffers with different concentrations of NaCl (0, 150, 500 mM). In the final experiment (500 mM NaCl), unlabeled p14arf-NoLS peptide was added at increasing concentrations up to 10 equivalents per NPM1-Nter monomer. Spectral changes were monitored by acquiring ^1H–^{15}N TROSY spectra after each addition. The backbone resonance assignment of NPM1-Nter (BMRB 19982) was transferred to the ^1H–^{15}N TROSY spectra; 92 of the 102 previously assigned residues were unambiguously reassigned and were included in the analysis. Signal intensity and chemical shift data were collected and analyzed as above.

SEC-MALS experiments

Size exclusion chromatography–MALS experiments were performed at room temperature on NPM1-Nter, either alone or in the presence of two equivalents of p14arf-NoLS peptide, in 20 mM phosphate buffer, pH 7.1, in the absence of NaCl. Denaturation experiments were performed with NPM1-Nter alone in 20 mM phosphate buffer pH 7.1 either without or with 4 M urea both in the protein sample and in the running buffer. In all experiments, a Superdex 200 10/30 column was used at a flow rate of 0.5 mL·min^{-1}, coupled to a Wyatt DAWN EOS light scattering detector, a Optilab rEX online refractometer, and a WyattQels DLS module. For each run, 200 μL of sample containing 200 μM NPM1-Nter was injected. The data were processed and analyzed with the ASTRA (Wyatt Technology, Santa Barbara, CA, USA) software.

Acknowledgements

The authors thank Dr. A. Gallo (University of Warwick, UK) for preliminary tests on p14arf. This work was partially supported by a grant from the Associazione Italiana Ricerca sul Cancro (IG2014-15197 to LF), by Instruct-ERIC, a Landmark ESFRI project, and specifically by the CERM/CIRMMP Italy Centre.

Conflict of interest

The authors declare that they have no conflicts of interest with the contents of this article.

Author contributions

EL, SC, ADM, MB, LB and LF designed research and analyzed the data. EL, SC, MF and ADM performed experiments. EL, MB, LB and LF wrote the manuscript.

References

1 Ozenne P, Eymin B, Brambilla E & Gazzeri S (2010) The ARF tumor suppressor: structure, functions and status in cancer. *Int J Cancer* **127**, 2239–2247.
2 Maggi LB Jr, Winkeler CL, Miceli AP, Apicelli AJ, Brady SN, Kuchenreuther MJ & Weber JD (2014) ARF tumor suppression in the nucleolus. *Biochim Biophys Acta* **1842**, 831–839.
3 Foulkes WD, Flanders TY, Pollock PM & Hayward NK (1997) The CDKN2A (p16) gene and human cancer. *Mol Med* **3**, 5–20.
4 Ruas M & Peters G (1998) The p16^{INK4a}/CDKN2A tumor suppressor and its relatives. *Biochim Biophys Acta* **1378**, F115–F177.
5 Saporita AJ, Maggi LB Jr, Apicelli AJ & Weber JD (2007) Therapeutic targets in the ARF tumor suppressor pathway. *Curr Med Chem* **14**, 1815–1827.
6 Kamijo T, Bodner S, van de Kamp E, Randle DH & Sherr CJ (1999) Tumor spectrum in ARF-deficient mice. *Cancer Res* **59**, 2217–2222.
7 Sherr CJ (2001) The INK4a/ARF network in tumour suppression. *Nat Rev Mol Cell Biol* **2**, 731–737.
8 Tao W & Levine AJ (1999) P19(ARF) stabilizes p53 by blocking nucleo-cytoplasmic shuttling of Mdm2. *Proc Natl Acad Sci USA* **96**, 6937–6941.
9 Grisendi S, Mecucci C, Falini B & Pandolfi PP (2006) Nucleophosmin and cancer. *Nat Rev Cancer* **6**, 493–505.

10 Colombo E, Alcalay M & Pelicci PG (2011) Nucleophosmin and its complex network: a possible therapeutic target in hematological diseases. *Oncogene* **30**, 2595–2609.
11 Federici L & Falini B (2013) Nucleophosmin mutations in acute myeloid leukemia: a tale of protein unfolding and mislocalization. *Protein Sci* **22**, 545–556.
12 Falini B, Mecucci C, Tiacci E, Alcalay M, Rosati R, Pasqualucci L, La Starza R, Diverio D, Colombo E, Santucci A *et al.* ; Acute Leukemia Working Party GIMEMA (2005) Cytoplasmic nucleophosmin in acute myelogenous leukemia with a normal karyotype. *N Engl J Med* **352**, 254–266.
13 Chiarella S, De Cola A, Scaglione GL, Carletti E, Graziano V, Barcaroli D, Lo Sterzo C, Di Matteo A, Di Ilio C, Falini B *et al.* (2013) Nucleophosmin mutations alter its nucleolar localization by impairing G-quadruplex binding at ribosomal DNA. *Nucleic Acids Res* **41**, 3228–3239.
14 Bertwistle D, Sugimoto M & Sherr CJ (2004) Physical and functional interactions of the Arf tumor suppressor protein with nucleophosmin/B23. *Mol Cell Biol* **24**, 985–996.
15 Sherr CJ (2006) Divorcing ARF and p53: an unsettled case. *Nat Rev Cancer* **6**, 663–673.
16 Korgaonkar C, Hagen J, Tompkins V, Frazier AA, Allamargot C, Quelle FW & Quelle DE (2005) Nucleophosmin (B23) targets ARF to nucleoli and inhibits its function. *Mol Cell Biol* **25**, 1258–1271.
17 Gjerset RA (2006) DNA damage, p14arf, nucleophosmin (NPM/B23) and cancer. *J Mol Histol* **37**, 239–251.
18 Colombo E, Martinelli P, Zamponi R, Shing DC, Bonetti P, Luzi L, Volorio S, Bernard L, Pruneri G, Alcalay M *et al.* (2006) Delocalization and destabilization of the Arf tumour suppressor by the leukemia-associated NPM mutant. *Cancer Res* **66**, 3044–3050.
19 Di Fiore PP (2008) Playing both sides: nucleophosmin between tumor suppression and oncogenesis. *J Cell Biol* **182**, 7–9.
20 Di Matteo A, Franceschini M, Chiarella S, Rocchio S, Travaglini-Allocatelli C & Federici L (2016) Molecules that target nucleophosmin for cancer treatment: an update. *Oncotarget* **7**, 44821–44840.
21 Mitrea DM, Grace CR, Buljan M, Yun MK, Pytel NJ, Satumba J, Nourse A, Park CG, Madan Babu M, White SW *et al.* (2014) Structural polymorphism in the N-terminal oligomerization domain of NPM1. *Proc Natl Acad Sci USA* **111**, 4466–4471.
22 DiGiammarino EL, Filippov I, Weber JD, Bothner B & Kriwacki RW (2001) Solution structure of the p53 regulatory domain of the p19Arf tumor suppressor protein. *Biochemistry* **40**, 2379–2386.
23 Bothner B, Lewis WS, DiGiammarino EL, Weber JD, Bothner SJ & Kriwacki RW (2001) Defining the molecular basis of Arf and Hdm2 interactions. *J Mol Biol* **314**, 263–277.
24 Menendez S, Khan Z, Coomber DW, Lane DP, Higgins M, Koufali MM & Lain S (2003) Oligomerization of the ARF tumor suppressor and its response to oxidative stress. *J Biol Chem* **278**, 18720–18729.
25 Szebeni A & Olson MO (1999) Nucleolar protein B23 has molecular chaperone activities. *Protein Sci* **8**, 905–912.
26 Mitrea DM, Cika JA, Guy CS, Ban D, Banerjee PR, Stanley CB, Nourse A, Deniz AA & Kriwacki RW (2016) Nucleophosmin integrates within the nucleolus via multi-modal interactions with proteins displaying R-rich linear motifs and rRNA. *Elife* **5**, e13571.
27 Di Matteo A, Franceschini M, Paiardini A, Grottesi A, Chiarella S, Rocchio S, Di Natale C, Marasco D, Vitagliano L, Travaglini-Allocatelli C *et al.* (2017) Structural investigation of nucleophosmin interaction with the tumor suppressor Fbw7γ. *Oncogenesis* **6**, e379.
28 Scott MS, Troshin PV & Barton GJ (2011) NoD: a Nucleolar localization sequence detector for eukaryotic and viral proteins. *BMC Bioinformatics* **12**, 317.
29 Zhang Y & Xiong Y (1999) Mutations in human ARF exon 2 disrupt its nucleolar localization and impair its ability to block nuclear export of MDM2 and p53. *Mol Cell* **3**, 579–591.
30 Bolli N, De Marco MF, Martelli MP, Bigerna B, Pucciarini A, Rossi R, Mannucci R, Manes N, Pettirossi V, Pileri SA *et al.* (2009) A dose-dependent tug of war involving the NPM1 leukaemic mutant, nucleophosmin, and ARF. *Leukemia* **23**, 501–509.
31 De Cola A, Pietrangelo L, Forlì F, Barcaroli D, Budani MC, Graziano V, Protasi F, Di Ilio C, De Laurenzi V & Federici L (2014) AML cells carrying *NPM1* mutation are resistant to nucleophosmin displacement from nucleoli caused by the G-quadruplex ligand TmPyP4. *Cell Death Dis* **5**, e1427.
32 Itahana K, Bhat KP, Jin A, Itahana Y, Hawke D, Kobayashi R & Zhang Y (2003) Tumor suppressor ARF degrades B23, a nucleolar protein involved in ribosome biogenesis and cell proliferation. *Mol Cell* **12**, 1151–1164.
33 Brady SN, Yu Y, Maggi LB Jr & Weber JD (2004) ARF impedes NPM/B23 shuttling in an Mdm2-sensitive tumor suppressor pathway. *Mol Cell Biol* **24**, 9327–9338.
34 Sivakolundu SG, Nourse A, Moshiach S, Bothner B, Ashley C, Satumba J, Lahti J & Kriwacki RW (2008) Intrinsically unstructured domains of Arf and Hdm2 form bimolecular oligomeric structures *in vitro* and *in vivo*. *J Mol Biol* **384**, 240–254.

35 Rizos H, Darmanian AP, Mann GJ & Kefford RF (2000) Two arginine rich domains in the p14ARF tumour suppressor mediate nucleolar localization. *Oncogene* **19**, 2978–2985.
36 Mitrea DM & Kriwacki RW (2012) Cryptic disorder: an order-disorder transformation regulates the function of nucleophosmin. *Pac Symp Biocomput* **2012**, 152–163.
37 Itahana K & Zhang Y (2008) Mitochondrial p32 is a critical mediator of ARF-induced apoptosis. *Cancer Cell* **13**, 542–553.
38 Tamiola K, Acar B & Mulder FA (2010) Sequence-specific random coil chemical shifts of intrinsically disordered proteins. *J Am Chem Soc* **132**, 18000–18003.